Mg-spinel lithology: A new rock type on the lunar farside

C. M. Pieters,[1] S. Besse,[2] J. Boardman,[3] B. Buratti,[4] L. Cheek,[1] R. N. Clark,[5] J. P. Combe,[6] D. Dhingra,[1] J. N. Goswami,[7] R. O. Green,[4] J. W. Head,[1] P. Isaacson,[1] R. Klima,[8] G. Kramer,[6] S. Lundeen,[4] E. Malaret,[9] T. McCord,[6] J. Mustard,[1] J. Nettles,[1] N. Petro,[10] C. Runyon,[11] M. Staid,[12] J. Sunshine,[2] L. A. Taylor,[13] K. Thaisen,[13] S. Tompkins,[14] and J. Whitten[1]

Received 30 August 2010; revised 27 January 2011; accepted 8 February 2011; published 22 April 2011.

[1] High-resolution compositional data from Moon Mineralogy Mapper (M^3) for the Moscoviense region on the lunar farside reveal three unusual, but distinctive, rock types along the inner basin ring. These are designated "OOS" since they are dominated by high concentrations of orthopyroxene, olivine, and Mg-rich spinel, respectively. The OOS occur as small areas, each a few kilometers in size, that are widely separated within the highly feldspathic setting of the basin rim. Although the abundance of plagioclase is not well constrained within the OOS, the mafic mineral content is exceptionally high, and two of the rock types could approach pyroxenite and harzburgite in composition. The third is a new rock type identified on the Moon that is dominated by Mg-rich spinel with no other mafic minerals detectable (<5% pyroxene, olivine). All OOS surfaces are old and undisturbed since basin formation. They are effectively invisible in image data and are only recognized by their distinctive composition identified spectroscopically. The origin of these unusual lithologies appears to be linked to one or more magmatic intrusions into the lower crust, perhaps near the crust-mantle interface. Processes such as fractional crystallization and gravity settling within such intrusions may provide a mechanism for concentrating the mafic components within zones several kilometers in dimension. The OOS are embedded within highly anorthositic material from the lunar crust; they may thus be near contemporaneous with crustal products from the cooling magma ocean.

Citation: Pieters, C. M., et al. (2011), Mg-spinel lithology: A new rock type on the lunar farside, *J. Geophys. Res.*, *116*, E00G08, doi:10.1029/2010JE003727.

1. Introduction

[2] The farside of the Moon has always been a mystery and is only accessible by spacecraft. New compositional information from the Moon Mineralogy Mapper (M^3) onboard Chandrayaan-1 has identified a suite of highly unusual rock types exposed at small areas within the farside Moscoviense Basin.

[3] The canonical compositional characterization of the lunar crust includes widespread feldspathic products of a magma ocean (ferroan anorthosite (FAN)), smaller pockets of near-contemporaneous magmatic rocks (Mg suite), and subsequent brecciation and redistribution of both by impact events, including those of the late heavy bombardment [e.g., *Shearer and Papike*, 2005; *Shearer et al.*, 2006]. This overview of crustal properties was formulated largely based on detailed analyses of the compositional and physical properties of lunar samples returned to Earth from the central lunar nearside by the Apollo and Luna missions, supplemented by data from a few dozen lunar meteorites. The perspectives from these lunar samples were extended to the rest of the Moon using remote compositional analysis as instruments on Earth-based telescopes improved and

[1]Deptartment of Geological Sciences, Brown University, Providence, Rhode Island, USA.
[2]Department of Astronomy, University of Maryland, College Park, Maryland, USA.
[3]Analytical Imaging and Geophysics LLC, Boulder, Colorado, USA.
[4]Jet Propulsion Laboratory, California Institute of Technology, Pasadena, California, USA.
[5]U.S. Geological Survey, Denver, Colorado, USA.
[6]Bear Fight Institute, Winthrop, Washington, USA.
[7]Physical Research Laboratory, ISRO, Ahmedabad, India.
[8]Johns Hopkins University Applied Physics Laboratory, Laurel, Maryland, USA.
[9]Applied Coherent Technology Corp., Herndon, Virginia, USA.
[10]NASA Goddard Space Flight Center, Greenbelt, Maryland, USA.
[11]Department of Geology, College of Charleston, Charleston, South Carolina, USA.
[12]Planetary Sciences Institute, Tucson, Arizona, USA.
[13]Planetary Geosciences Institute, University of Tennessee, Knoxville, Tennessee, USA.
[14]Defense Advanced Research Projects Agency, Arlington, Virginia, USA.

Copyright 2011 by the American Geophysical Union.
0148-0227/11/2010JE003727

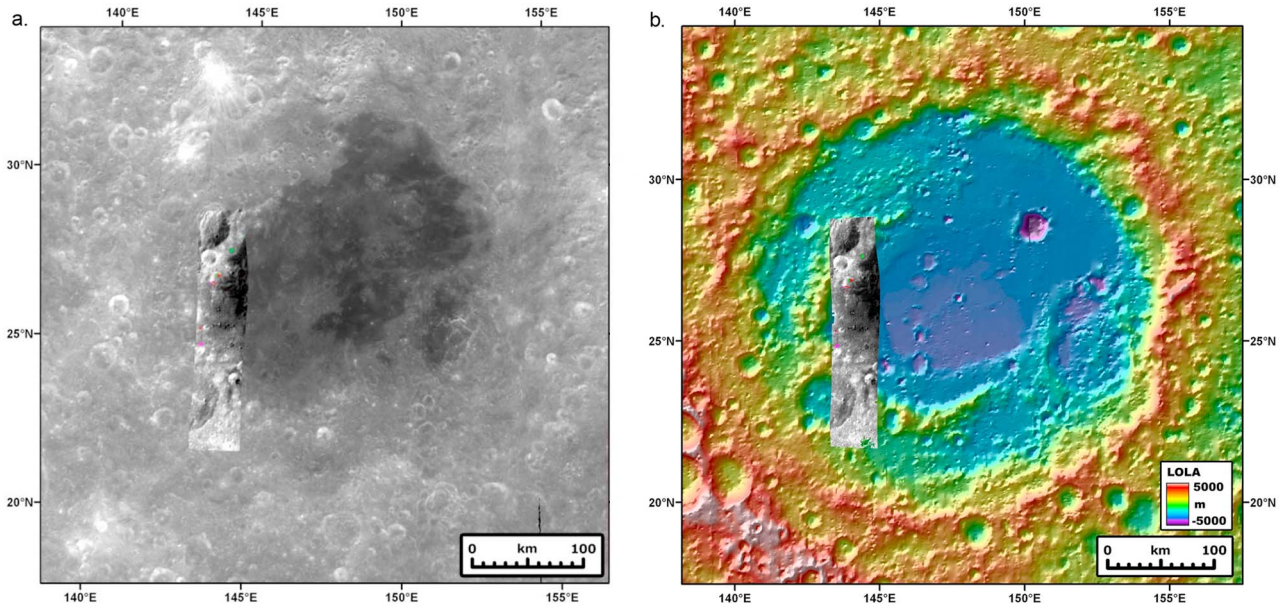

Figure 1. Moscoviense Basin on the lunar farside. (a) Clementine 750 nm albedo with M^3 orbit of data superimposed along the western inner ring (shown in detail in Figures 3, 4, and 6). (b) Topography of the basin as measured by LOLA on LRO.

instruments were eventually flown to study the Moon from orbit. An integrated study of remote data available in the last millennium identified three compositionally distinct lunar terranes: the nearside Procellarum KREEP Terrane (PKT), which exhibits high abundance of potassium, rare earth element, and phosphorus (KREEP), the farside Feldspathic Highland Terrane (FHT), and the mafic-rich farside terrane associated with the enormous South Pole–Aitken Basin (SPAT) [*Jolliff et al.*, 2000].

[4] By all accounts, the surface of the northern hemisphere of the lunar farside is one of the most feldspathic regions on the Moon, with a corresponding very low abundance of mafic minerals. The Moscoviense Basin (27°N, 146°E) occurs in this FHT region. It exhibits a well-developed, but asymmetric, ring system with the major topographic ring being 420 km in diameter [*Namiki et al.*, 2009]. An assessment of the geologic setting of Moscoviense Basin is given by *Thaisen et al.* [2011]. Unlike many other basins on the farside, the Moscoviense interior has been filled by a series of diverse mare basalts [e.g., *Craddock et al.*, 1997; *Kramer et al.*, 2008] with an emplacement history that spans almost 1.5 Gyr after basin formation [*Haruyama et al.*, 2009; *Morota et al.*, 2009].

[5] An overview of the Moscoviense Basin is shown in Figure 1. Topographic measurements of the basin coupled with direct measurements of local gravity variations indicate that this basin exhibits the thinnest residual crust among measured basins [*Ishihara et al.*, 2009]. By analogy with the well-preserved Orientale Basin, the innermost ring likely represents material uplifted and exposed from depth [e.g., *Cintala and Grieve*, 1998; *Head*, 2010].

2. M^3 Measurements

[6] The Moon Mineralogy Mapper (M^3) is a state-of-the-art visible and near-infrared imaging spectrometer that was a guest instrument on Chandrayaan-1, the Indian Space Research Organization's (ISRO) first mission to the Moon [*Goswami and Annadurai*, 2009]. The M^3 is a PI-led NASA Discovery program Mission of Opportunity selected for science value through the peer review process. The instrument was built at the Jet Propulsion Laboratory and is designed to measure accurately the diagnostic mineral absorption bands of solar radiation reflected from the lunar surface with a spatial resolution and coverage to provide geologic context. The instrument performed exceptionally well [*Green et al.*, 2011], even though nonnominal challenges were encountered in lunar orbit [*Boardman et al.*, 2011].

[7] In order to accommodate anticipated downlink limitations, M^3 was designed to operate in two modes. The wavelength range and spectral resolution of M^3 is shown in Figure 2 in comparison to typical lunar sample spectra. The optimum mode for science was to be full spatial resolution (600 cross track pixels at 70 m/pixel) and full spectral resolution (260 bands at 10 nm from ~400 to 3000 nm). Since only up to 25% of the Moon could be covered at full resolution during the nominal mission, a reduced resolution mode (140 m/pixel and 85 spectral bands) was to be used to acquire global coverage early in the mission for context. Almost all the data acquired by M^3 during the 10 months of Chandarayaan-1 operation was in the lower resolution Global Mode.

[8] As illustrated in Figure 2, mafic minerals such as pyroxenes and olivine exhibit a variety of highly diagnostic absorption bands near 1000 nm and 2000 nm due to ferrous iron that occurs in well-defined crystal structures [e.g., *Burns*, 1993; *Klima et al.*, 2007, 2008, 2011]. Although crystalline plagioclase can exhibit a feature near 1250 mm if it contains a few tenths of a percent FeO in its structure, the crystal structure of plagioclase and the observed absorption feature

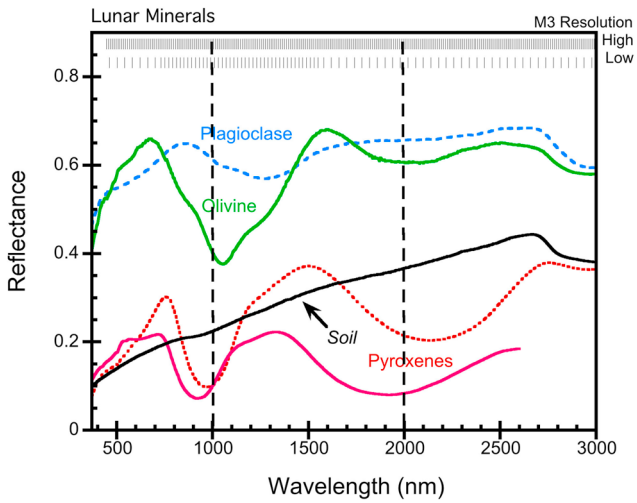

Figure 2. Reflectance spectra of lunar samples measured in Earth-based laboratory. Shown along the top are the M^3 channels for the full resolution mode (260 bands) and the lower-resolution global mode (85 bands). Dashed lines are drawn at 1000 and 2000 nm for comparisons with M^3 spectra. The feature at 2800–3000 nm is believed to be residual adsorbed terrestrial water.

are easily lost if the mineral experiences significant shock pressures [e.g., *Johnson and Hörz*, 2003]. Anorthosites or highly feldspathic rock types with <5% mafic minerals are thus relatively featureless and exhibit little if any mafic mineral signature at these wavelengths.

[9] The M^3 data presented and discussed here are extracted from an orbit of data taken early in the Chandrayaan-1 mission on 25 January 2009 (file M3G20090125T172601). The data were acquired as part of an extended test to evaluate the effects of the spacecraft thermal environment on M^3 and required the spacecraft to point slightly off nadir. The procedure was quite successful and nearly a full orbit of M^3 data was acquired across the western rim of the Moscoviense Basin. The location is shown in Figure 1. The average phase angle in the center of the M^3 strip at Moscoviense was 42°. Due to a severe thermal environment of the spacecraft, M^3 required a combination of preflight and in-flight calibration procedures. Calibration for M^3 level 1B radiance values are described by *Green et al.* [2011]. Part of the M^3 level 1B calibration included locating each M^3 picture element on the lunar surface utilizing a Lunar Orbiter Laser Altimetry (LOLA)-derived lunar reference frame. For a full description of M^3 instrument ray tracing and location on the lunar surface, see *Boardman et al.* [2011].

[10] In addition to standard processing and calibration for level 1 radiance data, version K [*Green et al.*, 2011], M^3 spectra discussed here have been evaluated using initial level 2 reflectance corrections. These include division by solar irradiance and a cos (i) correction. The resulting "apparent reflectance" contains small but systematic deviations that are corrected with a scalar "ground truth" correction factor to align them with known smooth properties of lunar soils. For this study, we have used an initial KRC1 for this correction described by *Clark et al.* [2011] as well as relative reflectance to minimize systematic errors.

[11] Three examples of image products of M^3 data for the Moscoviense region are shown in Figure 3. For Figure 3 (left), we have chosen to use 1489 nm (band 46 of the reduced resolution mode) to represent M^3 near-infrared albedo variations because this wavelength is not significantly involved with known mafic mineral absorptions and there is no thermal emission (only reflected solar radiation) in this part of the spectrum. Figure 3 (middle), integrated band depth (IBD) at 1000 nm is derived from 27 channels of M^3 data. A straight-line continuum is fit between 749 and 1579 nm. Band depth is computed for every channel from 789 to 1308 nm relative to this continuum, and IBD 1000 is their integrated value. In the IBD 1000 image of Figure 3 (middle), areas with strong mafic mineral absorptions near 1000 nm due to ferrous iron in the crystal structure appear bright; areas with weak or no mafic absorption appear as gray. Figure 3 (right), measured radiance at 2936 nm (band 84), contains a natural component of thermal emission radiation in addition to reflected solar radiation. Variations in surface temperature are particularly sensitive to small variations in local surface slope, and the combination of radiation at this wavelength enhances local morphology.

[12] Apart from the mare fill, the basin is highly feldspathic in overall character, consistent with its location in the FHT of *Jolliff et al.* [2000]. This is illustrated by the expansive gray region mapped with M^3 integrated band depth (IBD 1000) in Figure 3 that indicates the nonmare regions have undetectable amounts of mafic minerals. Even superimposed large craters such as Tereshkova (30 km crater near top of Figure 3) expose feldspathic materials. Representative spectra for the principal lithologies that dominate the basin are shown in Figure 4a. Highland soils and most large craters across the basin exhibit few, if any, detectible mafic minerals. A few prominent exceptions of local regions that contain mafic lithologies can be found further to the north at specific fresh craters along the Moscoviense Basin ring [see *Yamamoto et al.*, 2010; *Isaacson et al.*, 2011]. The Moscoviense mare fill is easily distinguished in the IBD 1000 image of Figure 3 (middle) because basalts have abundant mafic minerals, with pyroxenes dominating the spectral character. Spectra for mare soils and craters all exhibit absorptions due to the presence of iron-bearing minerals, although absorptions for soils are substantially subdued due to the alteration products of space weathering [e.g., *Pieters et al.*, 2000]. The characteristics of the mafic minerals that dominate mare basalts are best seen at fresh mare craters. For the two examples shown in Figure 4a the relatively long wavelength position of the ferrous absorptions near 1000 and 2000 nm indicates that augite (high-Ca pyroxene) is the dominant mafic mineral present, consistent with typical mare basalt mineralogy.

[13] A few small areas along the inner ring of the Moscoviense Basin deviate from the compositions seen in and around the basin. They were first noticed because they have unusually high or unusually low IBD 1000 relative to surrounding materials. As the region was evaluated with image processing techniques to identify unusual areas (e.g., principal component analyses) three unusual lithologies stood out at five areas (labeled 1–5 in Figure 4d). Spectra

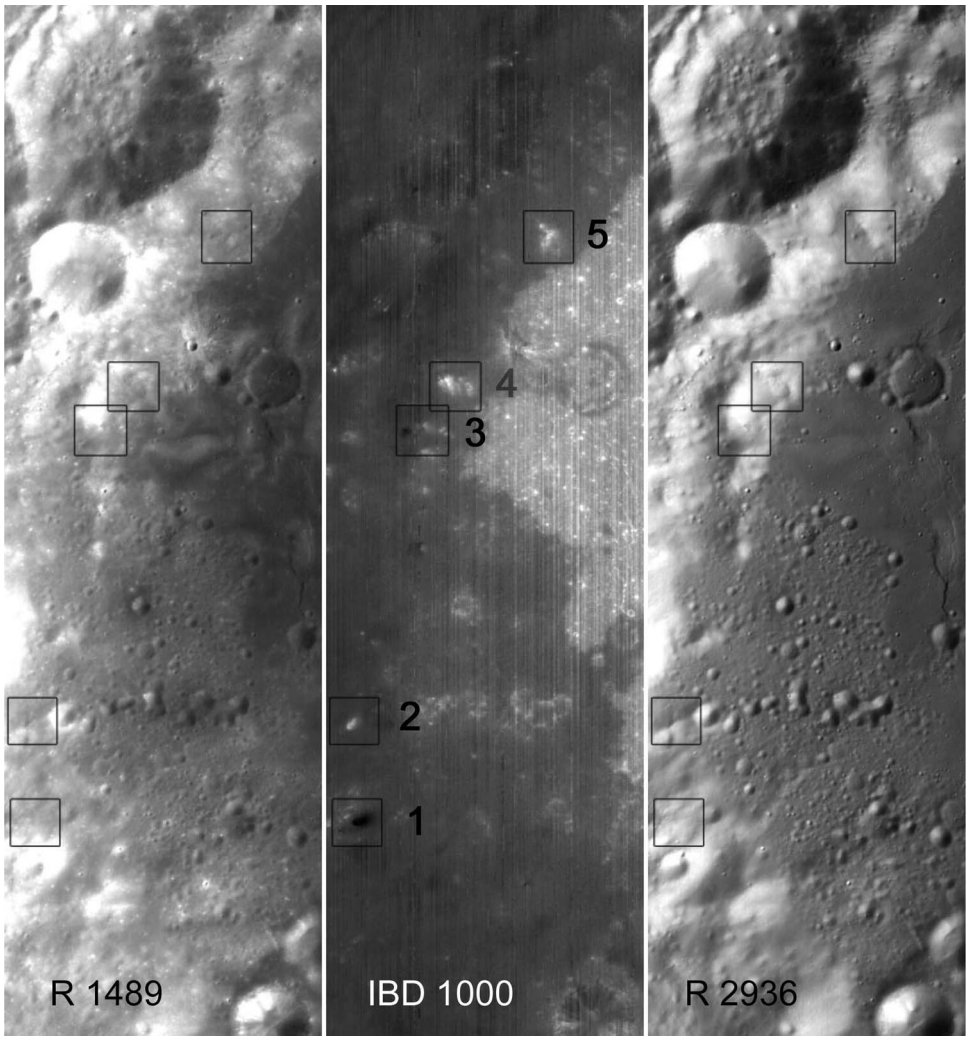

Figure 3. M^3 subscene across western Moscoviense Basin: (left) 1489 nm radiance, (middle) integrated band depth across 1000 nm, and (right) radiance at 2936 nm. Cross-track field of view is 40 km. OOS areas 1–5 (bottom to top) are centered in small boxes on each image. These regions are shown in higher spatial resolution in Figures 8–Figures 12.

collected from these five regions are shown in Figure 4b. Many of these spectra exhibit absorptions that appear to be as strong as those from fresh craters. Since all lunar spectra exhibit a relatively red continuum (increasing reflectance toward longer wavelengths), this continuum must be estimated and removed in order to evaluate the character of superimposed diagnostic mineral absorptions in more detail. The lunar continuum is poorly constrained, however, and there is no universally accepted way to do this. Typically, freshly exposed areas exhibit flatter continuum than well developed soils [e.g., *Pieters*, 1986, 1993]. For the Moscoviense region, these five usual areas appeared to exhibit a continuum slope comparable to many of the generally featureless spectra of well developed surrounding soils (compare Figures 4a and 4b). We thus chose to use one of these relatively featureless soil spectra (light blue in Figure 4a) as a reference. This procedure produced "relative reflectance spectra" (reflectance ratioed to the featureless soil spectrum) for the five unusual areas as shown in Figure 4c. This relative reflectance procedure has the advantage of also removing most residual instrumental artifacts.

3. OOS: Mineralogical Evaluation

[14] The five unusual regions exhibit remarkably consistent spectra, all quite different from local lithologies. They can be divided into three distinct rock type groups dominated by the following mafic minerals: (1) orthopyroxene, (2) olivine, and (3) Mg-Al spinel. We thus designate this family of unusual rock types as OOS. All are highly enriched in the dominant mafic mineral present; constraints on modal abundance for each are discussed in section 5.

3.1. Orthopyroxene

[15] The most readily identified OOS is the lithology dominated by orthopyroxene. It exhibits two relatively

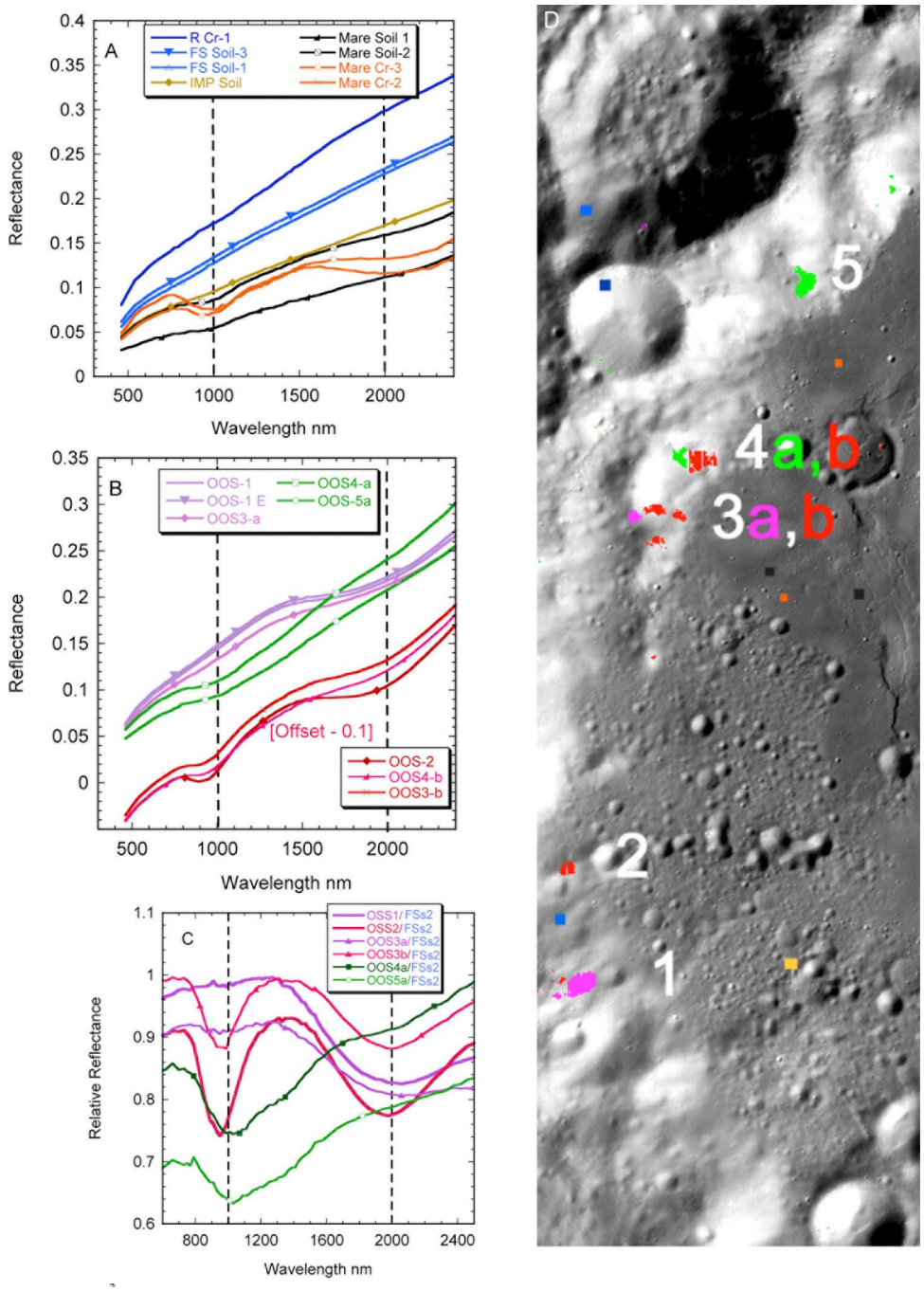

Figure 4. M^3 spectra: (a) Apparent reflectance local basin materials; (b) apparent reflectance of OOS regions; for clarity the orthopyroxene group is offset −0.1; and (c) relative reflectance spectra of OOS relative to a local featureless soil of similar albedo (blue in Figure 4a). Dashed lines are drawn at 1000 and 2000 nm to allow comparisons between Figures 4a, 4b, and 4c. (d) The locations of OOS are derived from principal component analyses and spectra selected for the center of each region. The locations of background spectra (Figure 4a) are shown with matching colors.

symmetric and well-defined absorptions. The absolute center of these bands is affected by the final calibrations to be used for M^3 data. Band minimum values in the relative reflectance spectra of Figure 4c occur near 940–950 nm and 1950–1970 nm. Shorter wavelengths are typically observed using radiance spectra with nominal solar calibration [see *Klima et al.*, 2011]. These coupled short band centers clearly fall into the range of low-Ca orthopyroxene [*Cloutis and Gaffey*, 1991; *Klima et al.*, 2008]. The type area for this lithology in Moscoviense is OOS 2, a small isolated area a few kilometers in dimension with no visible disturbance in M^3 images, such as an impact crater that might expose fresh

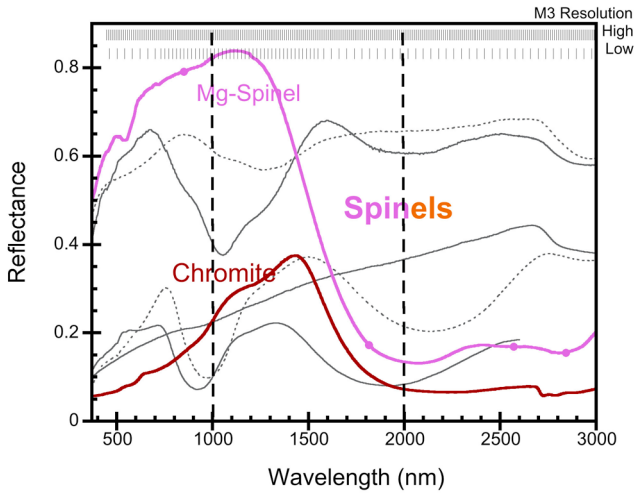

Figure 5. Reflectance spectra of spinels [from *Cloutis et al.*, 2004]. The background gray spectra are the common lunar minerals shown in Figure 2. All spinels exhibit a very strong electronic transition absorption near 2000 nm due to various amounts of Fe^{+2} in a tetrahedral site. Mg-rich spinels have little Fe^{+2} and are relatively bright and featureless across the 1000 nm region. The more iron-rich chromites are more absorbing in the visible and exhibit multiple absorptions due to transitions in Fe^{+2}, Cr^{+2}, and Cr^{+3}.

underlying material. This orthopyroxene-dominated lithology is shown in red in Figure 4.

3.2. Olivine

[16] The second distinct OOS rock type is shown in green in Figure 4. It exhibits a broad asymmetric absorption beyond 1000 nm with little, if any, feature near 2000 nm. These are classic properties of the presence of abundant olivine [e.g., *Sunshine and Pieters*, 1998], although additional mineral species are likely to be present such as plagioclase and possibly small amounts of pyroxene. Again, at widely separated locations the diagnostic features are distinct and repeatable. The areas themselves are spatially diffuse in M^3 data with no visible disturbance associated with crater ejecta or mass wasting at M^3 spatial resolution. Interestingly, these olivine-rich areas exhibit a steeper continuum than that of the surrounding soils.

3.3. Spinel

[17] The third OOS rock-type is new for the Moon. It has no detectable absorption feature near 1000 nm but exhibits a prominent absorption centered near 2000 nm. The Moscoviense type area is OOS 1, and this rock type is mapped as purple in Figure 4. Such distinctive near-infrared spectral properties have not been seen in remote measurements and have only been observed for isolated small lunar Mg-Al spinel as studied in thin section (e.g., sample 70002,7 of *Mao and Bell* [1975]). Reflectance spectra of terrestrial spinels [from *Cloutis et al.*, 2004] are shown in Figure 5. When ferric-bearing spinels are excluded, only the most Mg-rich spinels lack features near 1000 nm [e.g., *Cloutis et al.*, 2004]. Unlike the common lunar mafic minerals (pyroxene, olivine) that exhibit diagnostic crystal field absorption bands due to Fe^{+2} in distinctive octahedral sites, the strong broad absorption of spinels near 2000 nm is normally assigned to Fe^{+2} in a tetrahedral site [*Mao and Bell*, 1975; *Burns*, 1993]. Hence the absorption is very intense (due to the lack of a center of symmetry of the site). As with the other two OOS rock types, this newly detected Mg-spinel-dominated lithology exhibits no obvious or distinctive surface properties in images (such as fresh craters, bright streaks extending downslope, boulders, or outcrops) and occurs in the same form at widely separated sites (Figure 4). It is important to note that the lack of spectral features near 1000 nm for this OOS lithology provides a rigorous constraint on the maximum abundance of any pyroxene and olivine present. The M^3 observations require that the amount of any such mafic minerals be less than 5% for the Mg-spinel lithology, based on laboratory spectra and nonlinear mixing calculations. In contrast, Mg-spinel observed in lunar samples typically occurs with relatively abundant mafic minerals [e.g., *Prinz et al.*, 1973]. For example, a particularly spinel-rich sam-

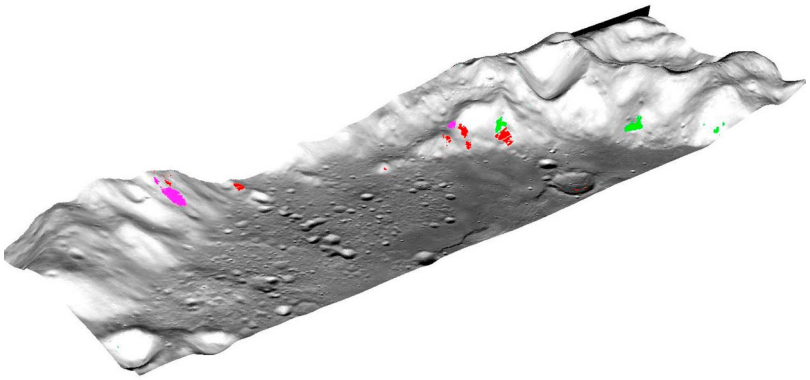

Figure 6. M^3 data for Moscoviense (2936 nm, band 84) in 3-D perspective using altimetry derived from LOLA data [see *Boardman et al.*, 2011]. The locations of OOS areas 1–5 are indicated with the same color as in Figure 4. Vertical exaggeration is ×5.

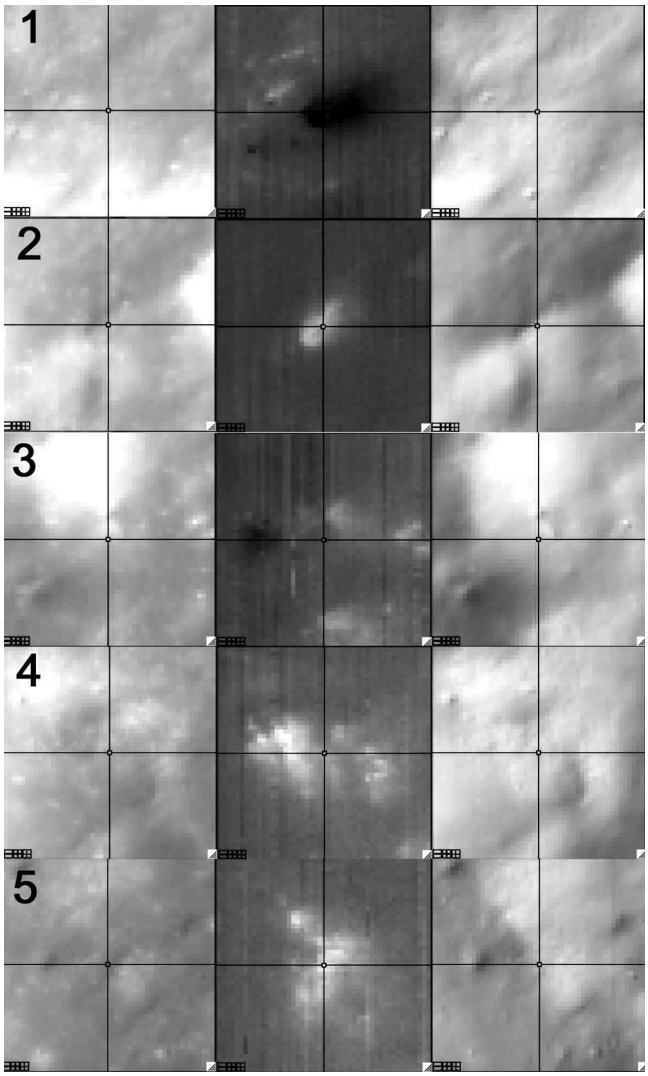

Figure 7. Close-up view of M^3 data for OOS areas 1–5 (box areas extracted from Figure 3 data). FOV across each image is ~7 km. (left) Radiance at 1489 nm; (middle) IBD 1000; and (right) radiance at 2936 nm. The crosshair is at the same location in each of the three images of OOS 1–5 for orientation only.

ple, spinel-troctolite 62295, contains ~6% spinel, but 25–28% olivine [e.g., *Walker et al.*, 1973a; *Ryder and Norman*, 1980].

3.4. Summary

[18] As described above, three unusual lithologies are detected along the inner ring of the Moscoviense Basin. These very distinctive compositions are localized, but exhibit diffuse boundaries and occur at widely separated locations with no apparent links between areas. In individual images, all OOS areas are morphologically indistinguishable from their surroundings. There is no physical marking within the resolution of M^3 that would indicate that anything unusual (e.g., primary impact craters, secondaries, outcrops of bedrock or large boulders, etc.) exists at these locations. It is only their composition derived from hyperspectral spectroscopy that identifies them as highly distinctive areas.

4. Possible Origins of OOS Lithologies

[19] Relying on these M^3 data, there are several options to consider for origin of the OOS. Possibilities fall into two classes: endogenic and exogenic.

4.1. Endogenic

[20] The most logical explanation for the origin of these three unusual lithologies is that the OOS represent products of processes that are or have been active on the Moon. If so, their origin must be tied to their location along the innermost ring of the Moscoviense impact basin. A 3-D perspective of OOS locations along this ring is shown in Figure 6. The OOS occur not along the steepest part of the ring, but in terrain across the base. The OOS might represent components of deeper crust uplifted and exposed by the basin-forming event itself. For example, the Mg suite of highland rocks found in the lunar sample collection, including gabbronorites, are thought to have formed early in crustal evolution from magmas that originated below the crust-mantle boundary and moved upward, assimilated, and otherwise incorporated various amounts of magma ocean products such as ferroan anorthosites into a plutonic system. During cooling of such plutonic systems, fractional crystallization and crystal settling would also form layered intrusives in the highland crust [e.g., *Raedeke and McCallum*, 1979, 1980]. The presence of fragments of the ancient Mg suite in the lunar sample collection suggests that such layered early intrusive plutons may be common [e.g., *James*, 1980]. Thus, excavation and exposure of different portions of deep-seated layered plutons is a viable hypothesis for the origin of the OSS outcrops observed at Moscoviense. As discussed below, this interpretation is our preferred origin for the OOS. The OOS presence, composition, and physical properties highlight a host of new issues, however, that need to be explored to understand the character and evolution of the lunar crust.

4.2. Exogenic

[21] Although unlikely, perhaps the OOS are derived from sources other than the Moon since their compositions relative to surroundings are very unusual. Diverse meteorites from across the Solar System frequently fall to Earth and identification of meteorites on the surface of Mars by the Mars Exploration Rovers [e.g., *Cromphaut et al.*, 2007] indicate that such foreign material can be found on other planetary surfaces. For both the Earth and Mars, however, the atmosphere plays a significant role in their deceleration and terminal velocity, and thus their preservation as coherent meteorites. For atmosphereless bodies, projectiles encounter the body at hypervelocities and the incoming projectiles are fragmented, vaporized, and dispersed during the impact event; only under very special circumstances might some of the impactor be retained [*Schultz and Gault*, 1985]. The individual compositions observed in OOS are known in meteorites [e.g., *Pieters and McFadden*, 1994], although these lithologies are not found together in known individual meteorites. One possible model for the origin of lunar OOS could be that they represent a strewn field of an asteroid

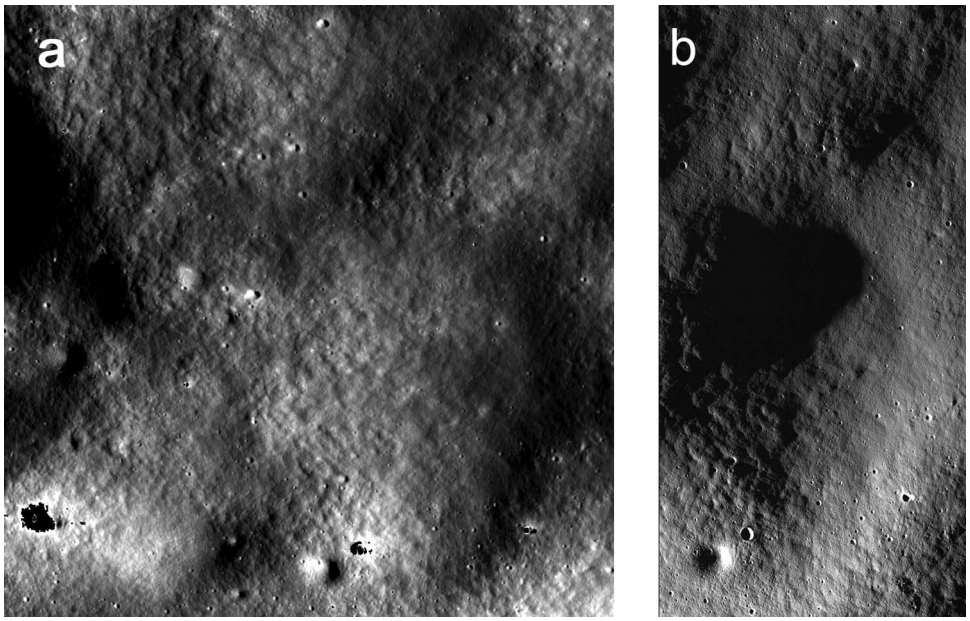

Figure 8. (a) SELENE TC and (b) LRO NAC images for OOS 1 area in Figure 7 at approximately the same scale. TC data have a few saturated pixels shown in black. LROC image is extracted from frame ID M103581557LC. NAC coverage only includes the right half of the Figure 7 image, and illumination is from the opposite direction.

rubble pile consisting of dispersed unrelated components of asteroidal material. This might be accomplished by the tidal breakup of a passing asteroid similar to the Shoemaker-Levy 9 series of events on Jupiter [e.g., *Hammel et al.*, 1995]. A string of such multiple special impact events could be consistent with the near-linear alignment of OOS 1–5, but large craters associated with their impact would have to have been erased.

5. Geologic Properties of OOS

[22] No visible disturbance, such as a crater, etc., was detected in association with the OOS at M^3 resolution (140 m/pixel). Although spectroscopy can often detect subpixel components with such well-defined properties [e.g., *Mustard and Sunshine*, 1999], it is valuable to investigate and validate the lack of such disturbance of the surface at ~15 times higher resolution to understand the OOS in geologic context with their surroundings. The international group of orbital lunar missions contained a variety of sensors designed to image the surface at a range of spatial resolution (with a single broad band). The Terrain Mapping Camera (TMC) on Chandrayaan-1 provides stereo imaging at a nominal 5 m/pixel [*Kumar et al.*, 2009]. The Terrain Camera (TC) on Kaguya provides stereo imaging at a nominal 10 m/pixel [*Haruyama et al.*, 2008]. The Narrow Angle Camera (NAC) on Lunar Reconnaissance Orbiter can obtain images with a scale as low as 0.5 m/pixel [*Robinson et al.*, 2010]. Each of the OOS areas has been imaged by one or more of these sensors, sometimes under different lighting conditions. Most such data are now available in the public domain. This additional high-resolution information can be used to further constrain the origin of the OOS.

5.1. Geologic Context at High Spatial Resolution

[23] An overview of the five OOS areas as seen in M^3 data is shown in Figure 7. The spatial resolution of M^3 is ~140 m/pixel, and for each subimage the field of view is ~7 km. The areal extent of each OOS is best seen in the middle IBD 1000 image (recall, the spinel-rich lithology appears dark and the orthopyroxene-rich and olivine-rich lithologies appear bright). The TMC camera was bore-sighted with M^3 on Chandrayaan-1. However, TMC has a narrower FOV than M^3, and as a result data for OOS 1 and 2 were not obtained.

[24] High-resolution images for OOS areas 1 and 2 were obtained by both TC and NAC. These are shown in Figures 8 and 9 for the areas outlined in Figure 7. For OOS 1 images the Sun angles were from opposite directions for TC and NAC. The NAC images can be examined in more detail at higher resolution, of course. The OOS 1 area is nevertheless completely invisible (indistinguishable) in these high spatial resolution data. The OOS 2 area appears to be associated with a small ridge near the base of the Moscoviense inner ring. Neither area exhibits an abundance of fresh craters or features that would otherwise expose underlying rocks. Both areas are dominated by well-developed (mature) soils across the region. At all available spatial scales, there is little in the local morphology to distinguish these OOS from any of their surroundings.

[25] Images for OOS areas 3, 4, and 5 were obtained by TMC at a higher Sun angle (lower incidence angle), i.e., less shadows, and are shown in Figures 10a, 10b, 11, and 12. For comparison, a NAC image of OOS area 3 obtained at a different illumination is shown in Figure 10b. Again, these three areas do not appear to have been involved with recent impact events or other geological processes mentioned

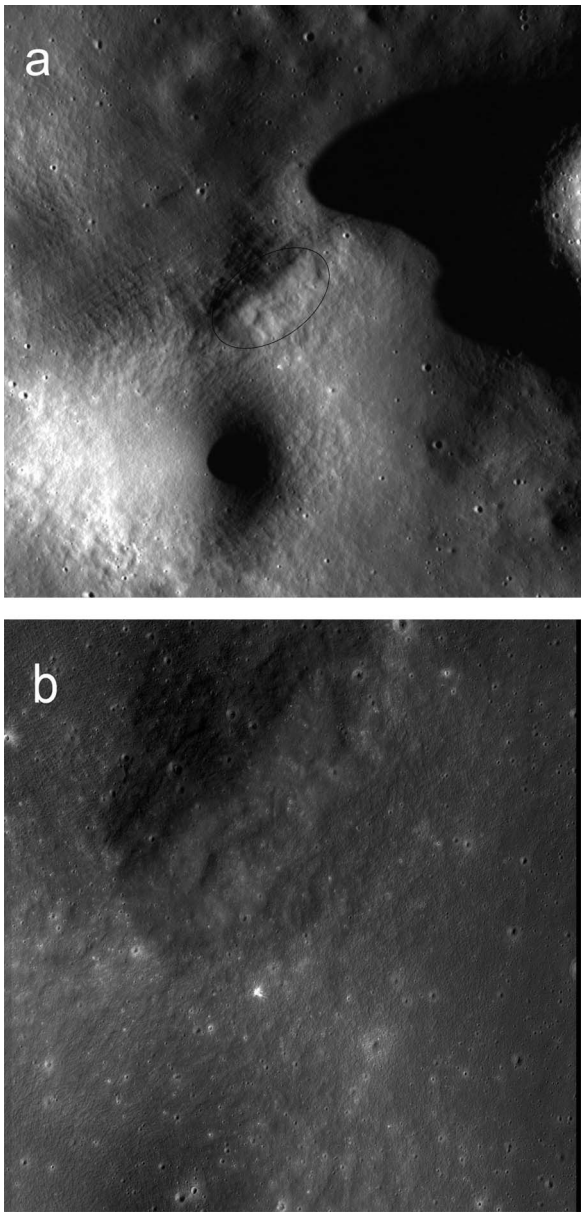

Figure 9. (a) SELENE TC and (b) LRO NAC images for OOS 2 area of Figure 7. The prime OOS 2 area is outlined by an oval in Figure 9a. The NAC image is approximately ×3 expanded scale and covers the central quarter of the OOS 2 region. LROC image is extracted from frame ID M113018261LC.

above, that would expose different underlying material at the OOS areas. There is nothing in the local morphology to distinguish these OOS from their surroundings.

5.2. Summary of Additional Properties

[26] Given the relative strength and prominence of the well-defined absorption features seen in M^3 OOS spectra (Figure 4), it was expected that the high-resolution data would uncover craters or local disturbance below the resolution of M^3. Well-developed soils contain alteration products that accumulate during extended exposure in the space environment (e.g., nanophase metallic iron) and significantly weaken any diagnostic absorption bands present [*Pieters et al.*, 2000; *Taylor et al.*, 2001, 2010]. The paradigm developed from extensive low spatial resolution telescopic measurements of the Moon is that strong absorption features are associated with local features such as craters or steep mountain slopes that have exposed fresh underlying materials that have not yet developed mature soils. The OOS are now exceptions to this general rule: they exhibit strong well-defined and diagnostic absorption bands while also maintaining well-developed soils on the surface.

[27] In addition to the compositional implications of M^3 spectra for the three distinct OOS lithologies discussed above, the high-resolution image data provide the following additional information about OOS properties:

[28] 1. All compositionally distinct OOS areas are indistinguishable from their surroundings in images at high spatial resolution. There are hints of albedo markings under some illumination geometries, but the data are insufficient to be definitive.

[29] 2. These unusual OOS lithologies along the Moscoviense Basin ring are not associated with a later local impact event. There is no evidence of recent disturbance or geologic processes that might have led to the exposure of fresh immature regolith.

[30] 3. All OOS surfaces appear *old*. That is to say, their soils are as well developed as other regional soils, implying they share the same history of exposure to the space environment in the time subsequent to the Moscoviense Basin forming event.

6. Discussion and Implications

[31] Several first-order implications come from the combined data for the OOS:

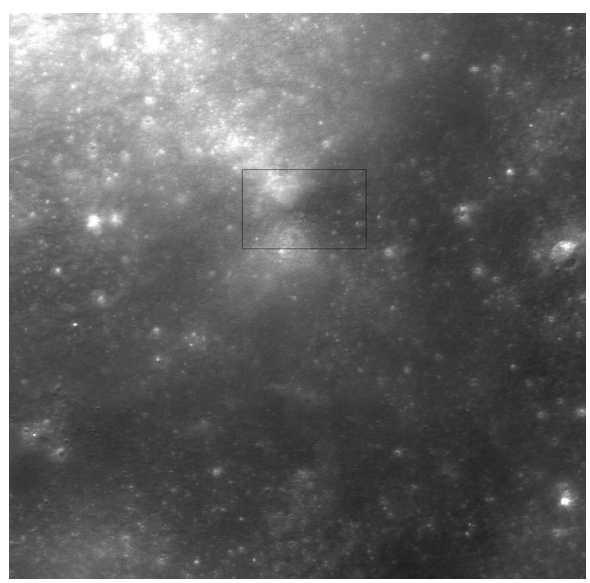

Figure 10a. Chandrayaan-1 TMC image for OOS 3 in Figure 7. These data were acquired at relatively high Sun. Rectangle outlines the area of NAC image in Figure 10b containing OOS 3b.

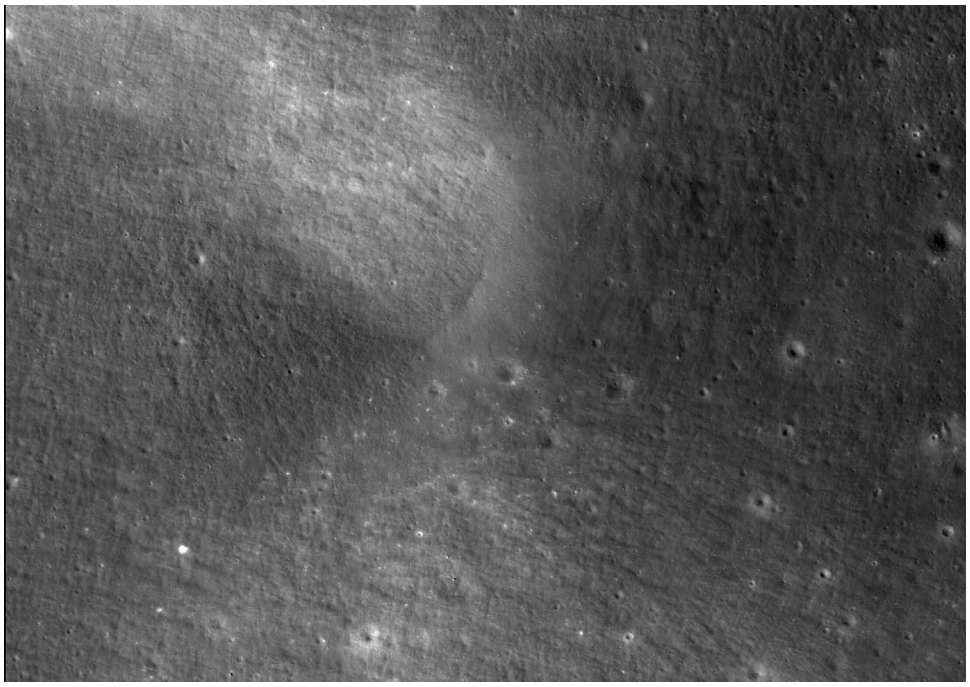

Figure 10b. Subimage of LROC NAC image M121267961LC centered on OOS 3b. The lower Sun angle allows the texture of the surface to be better seen.

[32] First, the OOS surfaces are old and appear to have remained in place undisturbed since the end of the modification stage following the Moscoviense Basin forming event. An exogenic origin for the unusual OOS materials is thus not possible. We prefer the interpretation that the OOS must represent components of the crust relocated by the Moscoviense event.

[33] Second, since the OOS surfaces have developed soils comparable to the well-developed soils seen elsewhere across the basin, the strength of their observed diagnostic absorption bands is an enigma. Their mineralogical implications are well defined (section 3), but their diagnostic bands are considerably stronger than any well-developed

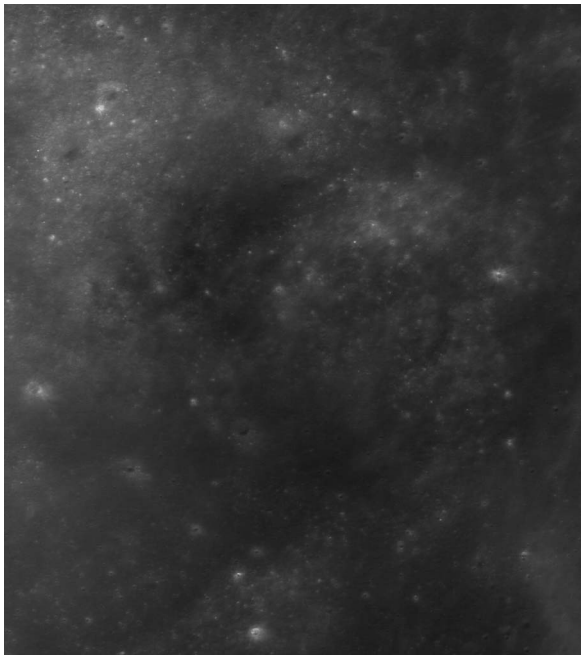

Figure 11. Chandrayaan-1 TMC image for OOS 4 in Figure 7.

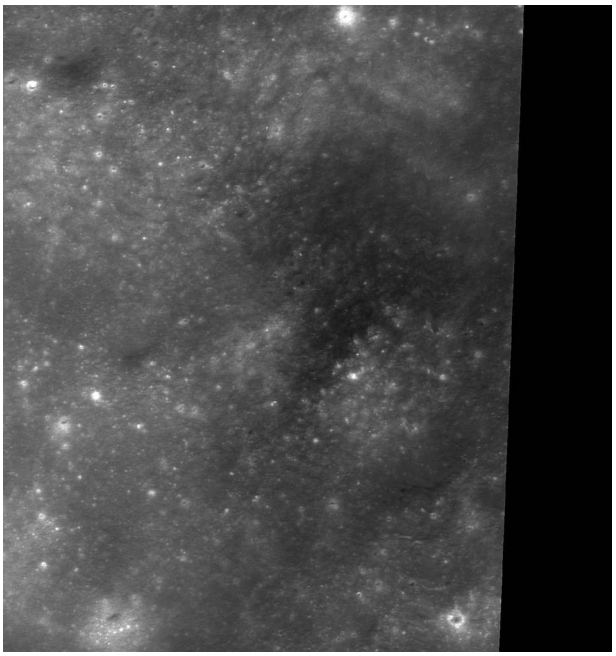

Figure 12. Chandrayaan-1 TMC image for OOS 5 in Figure 7.

(mature) soil observed previously with telescopic data or in the laboratory [e.g., *Taylor et al.*, 2001, 2010]. The absorptions are stronger than mare basalt soils (Figure 4b versus black lines of Figure 4a), which typically contain up to 50% mafic minerals. Either this entire region has not developed typical mature soils for a reason yet to be determined, or (more likely) the OOS areas contain an exceptionally high concentration of the absorbing species.

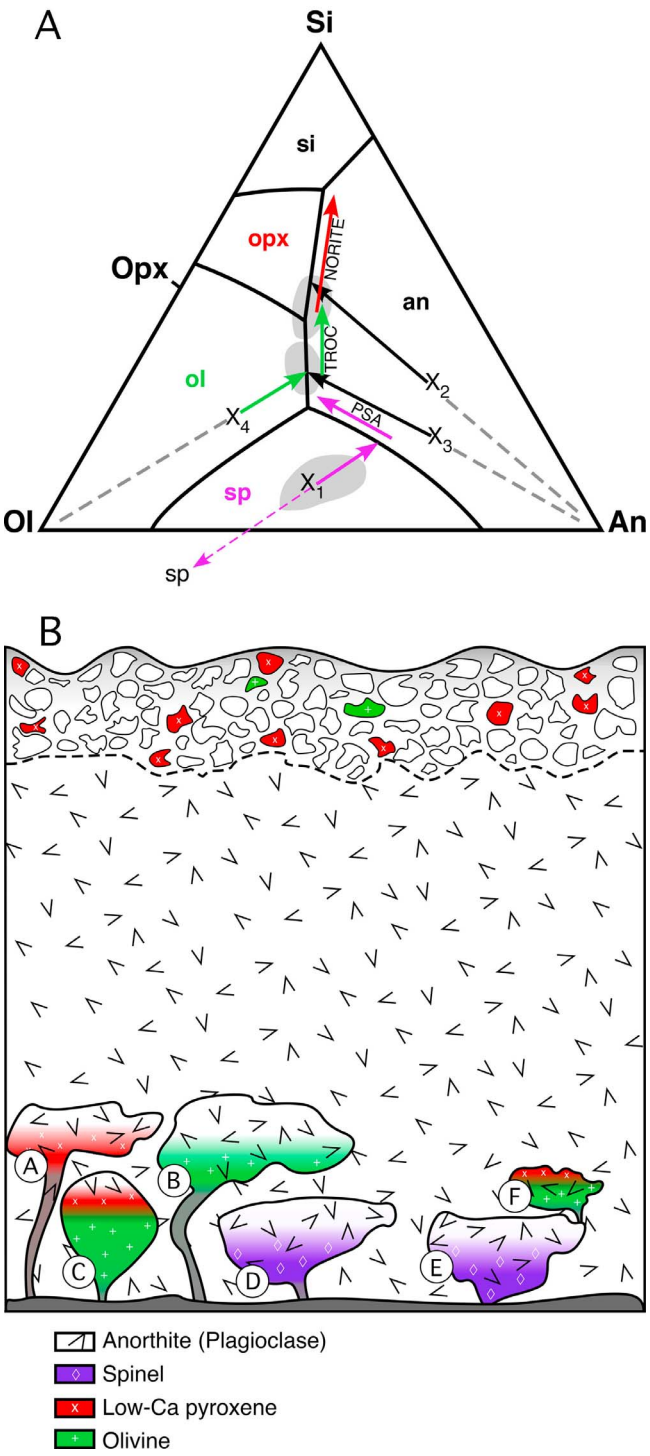

[34] We suggest that the OOS represent kilometer-scale expanses of mafic minerals more concentrated than normally seen. Fractional crystallization is one viable process to concentrate similar minerals during slow cooling of magma intrusions in the lower lunar crust [e.g., *McCallum and Schwartz*, 2001]. The exact mineral abundance is not yet known. The orthopyroxene-rich OOS lithology is clearly mafic-rich and could be a norite or gabbro-norite, and possibly a pyroxenite (plutonic rock of >90% pyroxene). Plagioclase content of the olivine-rich OOS lithology is unknown, but must be low to accommodate the band strength observed for the weathered surface. Within the resolution of M^3, small amounts of pyroxene may also be present. This rock type could be a troctolite trending to a dunite, or possibly a harzburgite (plutonic rock of olivine + orthopyroxene).

[35] The OOS spinel-rich lithology is a *new* rock type that has not yet been recognized in lunar samples. It contains abundant Mg-Al rich spinel (not chromite) and could be consistent with a spinel-anorthosite assemblage. However, it is important to note that the spinel separation from other mafic minerals is thorough, and this new rock type cannot contain more than 5% mafic minerals such as pyroxene or olivine.

[36] Third, we conclude from these analyses that billions of years of space weathering are insufficient to erase or hide small exposures of unusual rock types. With the advent of high spectral and high spatial resolution instruments, there is every expectation that similar exposures of material, both known and unusual, can be found across the entire surface of the Moon. Until now, we simply did not have the tools to

Figure 13. (a) Olivine-anorthite-silica pseudoternary commonly used to describe crystallization sequence for highland rocks [after *Walker et al.*, 1973b]. A trend of fractional crystallization involving olivine, anorthite, and pyroxene for several example initial melt compositions (X1, X2, X3, X4) is depicted. Since spinel is not an end-member of this pseudoternary, an arrow indicates the approximate compositional direction of spinel crystallization trends. The origins of possible melt compositions within the ternary have yet to be constrained (Mg- and Fe- rich are on the left, Al-rich on the right). OL, ol, olivine $(Mg, Fe)_2SiO_4$; An, an, anorthite $CaAl_2Si_2O_8$; Si, si, silica (SiO_2); Opx, opx, orthopyroxene $(Mg, Fe)_2SiO_3$; sp, spinel $(Mg, Fe)Al_2O_4$; PSA, pink spinel anorthosite; TROC, troctolite. (b) Schematic cross section for the Moscoviense region illustrating possible components of the deep lunar crust prior to the basin impact. The upper crust is dominantly anorthosite overlain by a megaregolith. The lower crust is more mafic. It may contain diverse magmatic plutons that exhibit a variety of compositions, several of which are observed as outcrops at Moscoviense. Although the relative portions of minerals present are unknown, several OOS exposures are highly enriched with mafic minerals, suggesting strong concentration (see text). Possible starting compositions (from Figure 13a) that might produce the mineralogy in these hypothetical plutons include: A (X2), B (X3), C (X4), D (X1 with crystallization before the melt reached the olivine field), E and F (X1 with two sequences of melt-crystal separation).

search for, characterize, and map small areas of distinctive highland rock types in their specific geologic context of emplacement.

[37] Fourth, high *spectral* resolution data are essential to characterize surface composition and identify distinctive rock types, and high *spatial* resolution data are critical to evaluate geologic context and the processes involved. The detection and characterization of OOS demonstrate that the Moon's compositional record can now be read in much more detail, and in geologic context, with the modern tools available.

7. Conclusions: Character of the Lunar Crust

[38] The Moscoviense Basin is an impact basin on the northern farside of the Moon with many classic morphologic and geologic properties. It has excavated deeply into a highly feldspathic crust and formed a series of concentric, but asymmetric basin rings [*Thaisen et al.*, 2011]. As a result the crust is extremely thin in this region [*Ishihara et al.*, 2009]. The basin interior has been filled by a series of diverse mare basalts over a period of a billion and a half years [*Haruyama et al.*, 2008; *Morota et al.*, 2009].

[39] Identified along the innermost Moscoviense Basin ring are several small exposures of three separate but distinctive rock types, the OOS, which contain an exceptionally high concentration of orthopyroxene, olivine, and Mg-rich spinel, respectively. The OOS rocks and developed soil have remained in place undisturbed along the Moscoviense ring since the basin formed.

[40] Crater models and geologic analyses predict that the innermost basin ring represents a zone of the deepest material displaced and exposed by the enormous basin-forming impact event [e.g., *Cintala and Grieve*, 1998; *Head*, 2010]. For the Moscoviense Basin, we believe the OOS represent components of the lower crust. The thin to non-existent crustal thickness estimates for the region [*Ishihara et al.*, 2009] suggest that the OOS zone of origin may even approach the crust-mantle interface.

[41] The three OOS lithologies are very distinctive and each occurs in more than one location. At the spatial scale of M^3 no clear gradients or mixing between OOS are observed. Although the OOS are widely dispersed along the inner ring, we have no direct information about any relationship between the three lithologies. All fade into background material within several pixels. There are cases where each appears completely separately from the others (OOS 1, 2, and 5). On the other hand, there are cases where the spinel lithology is spatially close to the orthopyroxene lithology (OOS 3) and where the orthopyroxene lithology occurs in close proximity to the olivine lithology (OOS 4), suggesting they may be genetically linked.

[42] We propose that the OOS are differentiation products of one or more plutonic events that intruded magmatic material into the lower part of the extensive feldspathic crust, itself derived from the magma ocean. The small size of the OOS (a few kilometers) suggest they could represent several separate small plutonic events or a large cooled plutonic body disrupted by the basin forming event. Illustrated in Figures 13 is a schematic cross section of the lunar crust prior to the impact that produced the Moscoviense Basin. At 4 Gyr the upper crust consisted largely of magma ocean products dominated by extensive ferroan anorthosite. To be consistent with the OOS observations, the lower crust contains diverse plutons which have undergone extensive fractionation resulting in relatively pure concentration of the three lithologies observed. The mineral concentration is massive, on a scale several kilometers in dimension. Currently, we do not know if separate plutons and their environment concentrated the olivine, the orthopyroxene, and the spinel or if the three lithologies represent a sequence of layers in a very large pluton disrupted by the impact event.

[43] We are confident of the characterization of the mineral compositions of the OOS. The position of OOS on the innermost ring of the Moscoviense Basin is evidence of their sampling from great depth. Their mineralogy is not consistent with upper crustal anorthositic material sampled by other basins (e.g., Orientale [*Pieters et al.*, 2009; *Head et al.*, 2010]), but rather strongly suggests that the Moscoviense Basin sampled down to lower crustal material. With the exception of the Mg-spinel lithology (which is new), the orthopyroxene- and olivine-rich mineralogy seen in OOS rock types are not unknown on the Moon. But they have never been seen in their actual geologic setting, nor in the concentrations implied by the M^3 data for OOS areas. Furthermore, as the remaining M^3 data are calibrated, additional outcrops of the Mg-spinel lithology have been also found at one other basin [*Dhingra et al.*, 2011], confirming that this new rock type plays a significant role in lunar crustal structure.

[44] This information provides important new insights and constraints on the character and evolution of early planetary crusts. This new compositional information about the lunar crust also opens new avenues of inquiry that are beyond the scope of the discussion presented here. What is the initial composition of melts that are needed to produce the three lithologies? How and when was the melt formed? What materials were melted? Where? How did the mineral separation and concentration occur at the scale observed? What size magma chamber is needed to allow such clear separation of lithologies as a layered intrusive? What depth? What temperature?

[45] These OOS results also provide a taste of major surprises that come from probing and analyzing data acquired by modern sensors orbiting the Moon. We have barely scratched the surface.

[46] **Acknowledgments.** M^3 is supported as a NASA Discovery Program mission of opportunity. These science results and science validation is supported through NASA contract NNM05AB26C. The M^3 team is honored to have had the opportunity to fly as a guest instrument on Chandrayaan-1, and we are grateful to all the ISRO team that enabled M^3 data to be returned. We gratefully acknowledge the valuable input to this project by the Chandrayaan-1 Terrain Mapping Camera team led by K. Kumar and by the public release of SELENE Terrain Camera data and LRO Narrow Angle Camera data. We appreciate the helpful review comments by Brad Jolliff.

References

Boardman, J. W., C. M. Pieters, R. O. Green, S. Lundeen, P. Varansi, J. Nettles, N. E. Petro, P. J. Isaacson, S. Besse, and L. A. Taylor (2011), Measuring moonlight: An overview of the spatial properties, lunar coverage, selenolocation and related level 1B products of the Moon Mineralogy Mapper, *J. Geophys. Res.*, doi:10.1029/2010JE003730, in press.

Burns, R. G. (1993), *Mineralogical Applications of Crystal Field Theory*, 2nd ed., 551 pp., Cambridge Univ. Press, New York, doi:10.1017/CBO9780511524899.

Cintala, M., and R. Grieve (1998), Scaling impact melting and crater dimensions: Implications for the lunar cratering record, *Meteorit. Planet. Sci.*, *33*, 889–912, doi:10.1111/j.1945-5100.1998.tb01695.x.

Clark, R. N., C. M. Pieters, R. O. Green, J. W. Boardman, and N. E. Petro (2011), Thermal removal from near-infrared imaging spectroscopy data of the Moon, *J. Geophys. Res.*, doi:10.1029/2010JE003751, in press.

Cloutis, E. A., and M. J. Gaffey (1991), Pyroxene spectroscopy revisited: Spectral-compositional correlations and relationship to geothermometry, *J. Geophys. Res.*, *96*, 22,809–22,826, doi:10.1029/91JE02512.

Cloutis, E. A., J. M. Sunshine, and R. V. Morris (2004), Spectral reflectance-compositional properties of spinels and chromites: Implications for planetary remote sensing and geothermometry, *Meteorit. Planet. Sci.*, *39*, 545–565, doi:10.1111/j.1945-5100.2004.tb00918.x.

Craddock, R. A., M. S. Robinson, B. R. Hawke, and A. S. McEwen (1997), Clementine-based geology of the Moscoviense Basin, lunar farside, *Proc. Lunar Planet. Sci. Conf.*, *28*, 265–266.

Cromphaut, C., V. G. Resende, E. Grave, and R. E. Vandenberghe (2007), Mossbauer study of Meridiani Planum, the first iron-nickel meteorite found on the surface of Mars by the MER Opportunity, *Meteorit. Planet. Sci.*, *42*, 2119–2123, doi:10.1111/j.1945-5100.2007.tb01012.x.

Dhingra, D., C. M. Pieters, J. W. Boardman, J. W. Head, P. J. Isaacson, L. A. Taylor (2011) Theophilus crater: Compositional diversity and geological context of Mg-spinel bearing central peaks, *Lunar Planet. Science*, *XLII*, Abstract 2388.

Goswami, J. N., and M. Annadurai (2009), Chandrayaan-1: India's first planetary science mission to the Moon, *Curr. Sci.*, *6*(4), 486–491.

Green, R. O., C. M. Pieters, J. Boardman, S. Lundeen, M. Staid, and the M3 Team (2011), The Moon Mineralogy Mapper data set delivered to the planetary data system and calibration and validation status, *Lunar Planet. Sci.*, *XLII*, Abstract 2089.

Hammel, H., et al. (1995), HST imaging of atmospheric phenomena created by the impact of comet Shoemaker-Levy 9, *Science*, *267*(5202), 1288–1296, doi:10.1126/science.7871425.

Haruyama, J., T. Matsunaga, M. Ohtake, T. Morota, C. Honda, Y. Yokota, M. Torii, and Y. Ogawa, and the LISM Working Group (2008), Global lunar-surface mapping experiment using the Lunar Imager/Spectrometer on SELENE, *Earth Planets Space*, *60*, 243–256.

Haruyama, J., et al. (2009), Long-lived volcanism on the lunar farside revealed by SELENE terrain camera, *Science*, *323*, 905–908, doi:10.1126/science.1163382.

Head, J. W. (2010), Transition from complex craters to multi-ringed basins on terrestrial planetary bodies: Scale-dependent role of the expanding melt cavity and progressive interaction with the displaced zone, *Geophys. Res. Lett.*, *37*, L02203, doi:10.1029/2009GL041790.

Head, J. W., et al. (2010), The Lunar Orientale Basin: Structure and crustal mineralogy from Chandrayaan-1 Moon Mineralogy Mapper (M^3) data, *Lunar Planet. Sci.*, *XLI*, Abstract 1030.

Isaacson, P. J., et al. (2011), Remote compositional analysis of lunar olivine-rich lithologies with Moon Mineralogy Mapper (M^3) spectra, *J. Geophys. Res.*, doi:10.1029/2010JE003731, in press.

Ishihara, Y., S. Goossens, K. Matsumoto, H. Noda, H. Araki, N. Namiki, H. Hanada, T. Iwata, S. Tazawa, and S. Sasaki (2009), Crustal thickness of the Moon: Implications for farside basin structures, *Geophys. Res. Lett.*, *36*, L19202, doi:10.1029/2009GL039708.

James, O. B. (1980), Rocks of the early lunar crust, *Proc. Lunar Planet. Sci. Conf.*, *11*, 365–393.

Johnson, J. R., and F. Hörz (2003), Visible/near-infrared spectra of experimentally shocked plagioclase feldspars, *J. Geophys. Res.*, *108*(E11), 5120, doi:10.1029/2003JE002127.

Jolliff, B. L., J. J. Gillis, L. A. Haskin, R. L. Korotev, and M. A. Wieczorek (2000), Major lunar crustal terranes: Surface expression and crust-mantle origins, *J. Geophys. Res.*, *105*(E2), 4197–4216, doi:10.1029/1999JE001103.

Klima, R. L., C. M. Pieters, and M. D. Dyar (2007), Spectroscopy of synthetic Mg-Fe pyroxenes I: Spin-allowed and spin-forbidden crystal field bands in the visible and near-infrared, *Meteorit. Planet. Sci.*, *42*, 235–253, doi:10.1111/j.1945-5100.2007.tb00230.x.

Klima, R. L., C. M. Pieters, and M. D. Dyar (2008), Characterization of the 1.2 μm M1 pyroxene band: Extracting cooling history from near-IR spectra of pyroxenes and pyroxene-dominated rocks, *Meteorit. Planet. Sci.*, *43*, 1591–1604, doi:10.1111/j.1945-5100.2008.tb00631.x.

Klima, R. L., et al. (2011), New insights into lunar petrology: Distribution and composition of prominent low-Ca pyroxene exposures as observed by the Moon Mineralogy Mapper (M^3), *J. Geophys. Res.*, doi:10.1029/2010JE003719, in press.

Kramer, G. Y., B. L. Jolliff, and C. R. Neal (2008), Distinguishing high-alumina mare basalts using Clementine UVVIS and Lunar Prospector GRS data: Mare Moscoviense and Mare Nectaris, *J. Geophys. Res.*, *113*, E01002, doi:10.1029/2006JE002860.

Kumar, A., et al. (2009), Terrain Mapping Camera: A stereoscopic high-resolution instrument on Chandrayaan-1, *Curr. Sci.*, *96*(4), 492–495.

Mao, H. K., and P. M. Bell (1975), Crystal-field effects in spinel: Oxidation states of iron and chromium, *Geochim. Cosmochim. Acta*, *39*(6–7), 865–874, doi:10.1016/0016-7037(75)90032-0.

McCallum, I. S., and J. M. Schwartz (2001), Lunar Mg suite: Thermobarometry and petrogenesis of parental magmas, *J. Geophys. Res.*, *106*, 27,969–27,983, doi:10.1029/2000JE001397.

Morota, T., et al. (2009), Mare volcanism in the lunar farside Moscoviense region: Implication for lateral variation in magma production of the Moon, *Geophys. Res. Lett.*, *36*, L21202, doi:10.1029/2009GL040472.

Mustard, J. F., and J. M. Sunshine (1999), Spectral analysis for Earth science investigations, in *Manual of Remote Sensing*, vol. 3, *Remote Sensing for the Earth Sciences*, edited by A. N. Rencz and R. A. Ryerson, pp. 251–306, John Wiley, New York.

Namiki, N., et al. (2009), Farside gravity field of the Moon from four-way Doppler measurements of SELENE (Kaguya), *Science*, *323*, 900–905, doi:10.1126/science.1168029.

Pieters, C. M. (1986), Composition of the lunar highland crust from near-infrared spectroscopy, *Rev. Geophys. Space Phys.*, *24*(3), 557–578, doi:10.1029/RG024i003p00557.

Pieters, C. M. (1993), Compositional diversity and stratigraphy of the Lunar crust derived from reflectance spectroscopy, in *Remote Geochemical Analysis: Elemental and Mineralogical Composition*, edited by C. Pieters and P. Englert, pp. 309–339, Cambridge Univ. Press, Cambridge, U. K.

Pieters, C. M., and L. A. McFadden (1994), Meteorite and asteroid reflectance spectroscopy: Clues to early solar system processes, *Annu. Rev. Earth Planet. Sci.*, *22*, 457–497, doi:10.1146/annurev.ea.22.050194.002325.

Pieters, C. M., L. A. Taylor, S. K. Noble, L. P. Keller, B. Hapke, R. V. Morris, C. C. Allen, D. S. McKay, and S. Wentworth (2000), Space weathering on airless bodies: Resolving a mystery with lunar samples, *Meteorit. Planet. Sci.*, *35*, 1101–1107, doi:10.1111/j.1945-5100.2000.tb01496.x.

Pieters, C. M., et al. (2009), Mineralogy of the lunar crust in spatial context: First results from the Moon Mineralogy Mapper (M^3), *Lunar Planet. Sci.*, *XL*, Abstract 2052.

Prinz, M., E. Dowty, K. Keil, and T. E. Bunch (1973), Spinel troctolite and anorthosite in Apollo 16 samples, *Science*, *179*, 74–76, doi:10.1126/science.179.4068.74.

Raedeke, L. D., and I. S. McCallum (1979) Fractionation in the Stillwater Complex: An analog for the lunar crust and mantle, paper presented at Conference on The Lunar Highlands Crust, Lunar Sci. Inst., Houston, Tex.

Raedeke, L. D., and I. S. McCallum (1980), A comparison of fractionation trends in the lunar crust and the Stillwater complex, in *Lunar Highlands Crust*, edited by R. B. Merrill and J. J. Papike, pp. 133–153, Pergamon, New York.

Robinson, M. S., et al. (2010), Lunar Reconnaissance Orbiter Camera (LROC): Instrument overview, *Space Sci. Rev.*, *150*, 81–124, doi:10.1007/s11214-010-9634-2.

Ryder, G. and M. D. Norman (1980) *Catalog of Apollo 16 Rocks*, 3 vols., *Curator*'s *Off. Publ. 52*, Johnson Space Cent., Houston, Tex.

Schultz, P. H., and D. E. Gault (1985), Clustered impacts: Experiments and implications, *J. Geophys. Res.*, *90*, 3701–3732, doi:10.1029/JB090iB05p03701.

Shearer, C. K., and J. J. Papike (2005), Early crustal building processes on the Moon: Models for the petrogenesis of the magnesian suite, *Geochim. Cosmochim. Acta*, *69*, 3445–3461, doi:10.1016/j.gca.2005.02.025.

Shearer, C. K., et al. (2006), Thermal and magmatic evolution of the Moon, in *New Views of the Moon*, *Rev. Mineral. Geochem.*, vol. 60, edited by B. Jolliff et al., pp. 365–518, Mineral. Soc. of Am., Reston, Va.

Sunshine, J. M., and C. M. Pieters (1998), Determining the composition of olivine from reflectance spectroscopy, *J. Geophys. Res.*, *103*, 13,675–13,688, doi:10.1029/98JE01217.

Taylor, L. A., C. M. Pieters, L. P. Keller, R. V. Morris, and D. S. McKay (2001), Lunar mare soils: Space weathering and the major effects of surface-correlated nanophase Fe, *J. Geophys. Res.*, *106*, 27,985–28,999, doi:10.1029/2000JE001402.

Taylor, L. A., C. Pieters, A. Patchen, D.-H. S. Taylor, R. V. Morris, L. P. Keller, and D. S. McKay (2010), Mineralogical and chemical characterization of lunar highland soils: Insights into the space weathering of soils on airless bodies, *J. Geophys. Res.*, *115*, E02002, doi:10.1029/2009JE003427.

Thaisen, K. G., J. W. Head, L. A. Taylor, G. Y. Kramer, P. Isaacson, J. Nettles, N. Petro, and C. M. Pieters (2011), Geology of the Moscoviense Basin, *J. Geophys. Res.*, doi:10.1029/2010JE003732, in press.

Walker, D., J. Longhi, T. Grove, E. Stolper, and J. F. Hays (1973a) Experimental petrology and origin of rocks from the Descartes Highlands, *Proc. Lunar Sci. Conf.*, *4*, 1013–1032.

Walker, D., T. L. Grove, J. Longhi, E. M. Stolper, and J. F. Hays (1973b), Origin of lunar feldspathic rocks, *Earth Planet. Sci. Lett.*, *20*, 325–336, doi:10.1016/0012-821X(73)90006-X.

Yamamoto, S., et al. (2010), Possible mantle origin of olivine around lunar impact basins detected by SELENE, *Nat. Geosci.*, *3*, 533–536, doi:10.1038/ngeo897.

S. Besse and J. M. Sunshine, Department of Astronomy, University of Maryland, College Park, MD 20742-2421, USA.

J. Boardman, Analytical Imaging and Geophysics LLC, 4450 Arapahoe Ave., Ste. 100, Boulder, CO 80305, USA.

B. Buratti and S. Lundeen, Jet Propulsion Laboratory, California Institute of Technology, 4800 Oak Grove Dr., MS 183-401, Pasadena, CA 91109, USA.

L. Cheek, D. Dhingra, J. W. Head, P. Isaacson, J. Mustard, J. Nettles, C. M. Pieters, and J. Whitten, Department of Geological Sciences, Brown University, Box 1846, Providence, RI 02912, USA. (carle_pieters@Brown.edu)

R. N. Clark, U.S. Geological Survey, MS964, Box 25046, Federal Center, Denver, CO 80225, USA.

J. P. Combe, G. Kramer, and T. McCord, Bear Fight Institute, 22 Fiddler's Rd., Box 667, Winthrop, WA 98862, USA.

J. N. Goswami, Physical Research Laboratory, ISRO, NAVRANGPURA/THALTEJ, Ahmedabad 380009, India.

R. O. Green, Jet Propulsion Laboratory, California Institute of Technology, 4800 Oak Grove Dr., MS 306-438, Pasadena, CA 91109-8099, USA.

R. Klima, Johns Hopkins University Applied Physics Laboratory, 11100 Johns Hopkins Rd., Laurel, MD 20732-0000, USA.

E. Malaret, Applied Coherent Technology Corp., 112 Elden St., Ste. K, Herndon, VA 22070, USA.

N. Petro, NASA Goddard Space Flight Center, Code 698, Greenbelt, MD 20771, USA.

C. Runyon, Department of Geology, College of Charleston, 66 George St., Charleston, SC 29424, USA.

M. Staid, Planetary Science Institute, 1700 E. Fort Lowell, Ste. 106, Tucson, AZ 85719, USA.

L. A. Taylor and K. Thaisen, Planetary Geosciences Institute, Department of Earth and Planetary Sciences, University of Tennessee, 1412 Circle Dr., Knoxville, TN 37996-1410, USA.

S. Tompkins, Defense Advanced Research Projects Agency, 3701 N. Fairfax Dr., Arlington, VA 22203-1714, USA.